Title

Nano- and Mesoscale Ion and Water Transport in Perfluorosulfonic-Acid Membranes

Journal

ECS Transactions, 80(8)

ISSN

1938-5862

ISBN

978-1-62332-477-3

Authors

Crothers, Andrew Robert

Radke, Clayton J

Weber, Adam Z

Publication Date

2017-08-24

DOI

10.1149/08008.0593ecst

Peer reviewed

Nano- and Mesoscale Ion and Water Transport in Perfluorosulfonic-Acid Membranes

A. R. Crothers[a,b], C. J. Radke[a,b], A. Z. Weber[a]

[a]Lawrence Berkeley National Laboratory, Berkeley, CA 94720, USA
[b]Department of Chemical and Biomolecular Engineering, University of California, Berkeley, CA 94720, USA

Water and aqueous cations transport along multiple length scales in perfluorosulfonic-acid membranes. Molecular interactions in hydrophilic domains dictate nanoscale resistances while the connectivity of domains controls mesoscale transport. The developed multiscale models probes the synergy of these length scales. Concentrated solution theory and electrokinetics are used to predict transport in the aqueous domains as a function of hydration. A resistor network upscales the nanoscale properties to predict effective membrane ion and water transport and their coupling. The nature of macroscopic and nanoscale properties differs drastically because the mesoscale network mediates transport. Moreover, the effective tortuosity and connectivity is not the same for water and ion transport. The methodology and findings highlight improvement opportunities for membrane performance.

Introduction

The mass-transport properties of ion-conducting membranes prescribe performance of polymer-electrolyte fuel cells (PEFCs) (1). Chiefly, effective PEFC operation necessitates high membrane ionic conductivity (1). Because conductivity strongly increases with membrane hydration, rapid ion transport requires ample water content (1). Therefore, water diffusivity concomitantly controls conductivity for heterogeneous PEFC humidification by promoting thorough hydration in PEFCs (1). Water gradients also directly induce ionic current via transport couplings in which water convection and diffusion cause ion transport (e.g., electro-osmosis) (1-2). Improved membrane design and operation, consequently, require the simultaneous optimization of ion conductivity, water diffusivity, and their coupling (1). In this work, we present a model for mass transport of water and ions in PEFC membranes based on nanoscale properties that provides a framework to understand mesoscale membrane performance.

Prototypical PEFC membrane materials are perfluorinated sulfonic-acid ionomers (PFSA) (3). They are random co-polymers consisting of perfluorinated, Teflon-like backbones with pendant sidechains that terminate in sulfonic-acid groups (3). Hydrophobicity differences between the backbone and sidechains cause nanophase separation (3), wherein an inert hydrophobic matrix envelops hydrophilic domains

containing water and sulfonic-acid groups (3). The hydrophobic matrix ensures structural stability and durability (3). The sulfonic-acid proton transfers to a water molecule in the hydrophilic phase forming a hydronium ion (3). Additional water dissociates the hydronium from the sulfonate group (3). Proton movement carries ionic current through the nanoscale hydrophilic domains. These domains connect in a network at the mesoscale that provides a percolating pathway for transport across the membrane (3).

Because transport occurs across multiple lengthscales, improving membrane design requires concerted optimization at each lengthscale (3). Nevertheless, modeling efforts have either focused on macroscopic transport without grounding parameters in nanoscale phenomena or, conversely, studied the nanoscale without explicit connection to macroscale experiments, with a few exceptions (4-5).

We present a methodology to connect directly nanoscale properties with macroscopic ion and water transport and their coupling using an explicit representation of the conductive network. The mesoscale is represented by a resistor network for species transport. Two transport parameters describe water and ion mobility and another accounts for coupling between the two; each of these parameters are functions of water content. Conductances are calculated using a simple nanoscale model. The network model predicts macroscopic conductivity, water diffusivity, and electro-osmotic coefficient as a function of water content, enabling comparison to experimental data.

Theory

Mesoscale Transport

The connected aqueous domains of the PFSA membrane are treated as a resistor network. Each domain is a conductive element for transport and nodes of the network connect multiple domains. Concentrated-solution theory dictates that the difference, Δ, of water chemical potential, μ_{w}, and ionic potential (i.e. the electrochemical potential of protons), Φ, between two neighboring nodes a and b induce ionic current, $i^{a,b}$, and water flux, $N_{\mathrm{w}}^{a,b}$, through each aqueous slit domain of length L (4, 6)

$$i^{a,b} = -\kappa \frac{\Delta\Phi}{L} - \frac{\kappa\xi}{F}\frac{\Delta\mu_{\mathrm{w}}}{L} \qquad [1]$$

$$N_{\mathrm{w}}^{a,b} = -\frac{\kappa\xi}{F}\frac{\Delta\Phi}{L} - \left(\alpha + \frac{\kappa\xi^2}{F^2}\right)\frac{\Delta\mu_{\mathrm{w}}}{L} \qquad [2]$$

where F is Faraday constant. The current density is proportional to the flux of cations, $N_{+}^{a,b}$, (i.e. $i^{a,b} = FN^{a,b}$) because the anion is immobile and the cation has unity valance. The conductivity of the network element domain, κ, relates current to the ionic-potential difference. The water transport coefficient, α, relates water flux to a chemical potential

difference. The electro-osmotic coefficient, ξ, describes the coupling between water flux and current (3). Absent any concentration gradients, the conductivity, κ, is

$$\kappa = -\frac{i^{\alpha,\beta}}{\frac{\Delta\Phi}{\mathrm{L}}} \quad \text{for } \Delta\mu_{\mathrm{w}} = 0 \qquad [3]$$

The electro-osmotic coefficient, ξ, is the number of water molecules that accompany proton flux (absent concentration gradients)

$$\xi = \frac{N_{\mathrm{w}}^{\alpha,\beta}}{N_{+}^{\alpha,\beta}} \quad \text{for } \Delta\mu_{\mathrm{w}} = 0 \qquad [4]$$

Finally, the water transport coefficient relates the flux of water to its chemical potential gradient when there is no current

$$\alpha = -\frac{N_{\mathrm{w}}^{\alpha,\beta}}{\frac{\Delta\mu_{\mathrm{w}}}{L}} \quad \text{for } i^{a,b} = 0 \qquad [5]$$

The conductivity and electro-osmotic and water-transport coefficients of an aqueous domain element depend on water content, quantified by the molar ratio of water to sulfonate groups, λ (mole H_2O/ mole SO_3^-). The water content of an aqueous domain element, λ, is the macroscopic average (mean) water content, $\langle\lambda\rangle$, with some deviation from the mean, e_λ, caused by local variations in sulfonate-group concentration and polymer morphology

$$\lambda = \langle\lambda\rangle(\mu_{\mathrm{w}}) + e_\lambda \qquad [6]$$

where the mean of e_λ is zero and $\langle\lambda\rangle$ is a known function of water chemical potential (3).

The mesoscale transport system is fully specified at steady-state with species conservation. The fluxes of water and protons through each domain element into a node a from all neighboring nodes b satisfy (6)

$$\sum_b i^{a,b} = 0 \qquad [7]$$

and

$$\sum_b N_{\mathrm{w}}^{a,b} = 0 \qquad [8]$$

Equations 1, 2, 7, and 8 constitute a nonlinear system of equations because conductivity and the electro-osmotic and water-transport coefficients are functions of water chemical potential via Equation 6. Nanoscale physics governs the dependence of transport coefficients on water content.

Nanoscale Transport

The transport properties of the aqueous domain elements are linked to the local water content and nanoscale properties via a model of ion and water transport in the aqueous slit-like domains of a PFSA. The hydrophilic domains are strongly phase separated from the polymer backbone and are locally flat, ribbon-like channels (3). We idealize a domain as a slit filled with water and dissociated aqueous protons. The polymer, pendant sulfonate groups, and undissociated protons constitute the walls of the channel. The transport properties of a network element resistor include both the conducting aqueous slit and the associated insulating hydrophobic matrix.

Mass flux through a network resistor, $n_i = N_i/M_i$, is the mass flow of species i with molar mass M_i through the aqueous slit divided by the area of that slit and the enveloping polymer matrix. (The fluxes are treated as scalar since they occur bidirectionally along the channel). Total flux is the sum of convective and diffusive contributions

$$n_i = j_i + \varphi_{\mathrm{w}} \rho_i v \qquad [9]$$

where j_i is the diffusive mass flux, φ_{w} is the water volume fraction, v is the mass-averaged velocity, and ρ_i is the mass-density of species i ($+$ for protons and w for water) in the aqueous solution (7). The factor of φ_{w} normalizes the convective flux over the hydrophilic and hydrophobic areas of the resistor. According to the definition of the diffusive flux in a binary system, proton and water diffusive fluxes sum to zero in each domain element, i.e. $j_+ = -j_{\mathrm{w}}$ (7).

Absent concentration gradients, the diffusive flux of protons is proportional to the electrostatic gradient

$$j_+ = -\varphi_{\mathrm{w}} \rho_+ u_+ F \nabla \Phi \qquad [10]$$

where ρ_+ and u_+ are the density and mobility of dissociated protons in the aqueous domain, respectively (7). As in Equation 9, φ_{w} corrects for the conductive volume fraction. Upon distributing the dissociated protons uniformly across the aqueous domain, the electrostatic Hagen-Poiseuille equation gives the average velocity in that aqueous slit element (7)

$$v = -\frac{h^2}{12\eta}(c_+ F \nabla \Phi) \qquad [11]$$

for laminar flow, where h is the height of the slit, η is the viscosity of the solution, and c_+ $(= \rho_+/M_+)$ is the molar concentration of dissociated protons (7). The electrostatic body force on the dissociated protons (the term in parenthesis) replaces the pressure gradient of the classic Hagen-Poiseuille equation (7).

Substitution of Equations 9 thru 11 into Equation 3 relates the conductivity to nanoscale properties

$$\kappa = \varphi_{\mathrm{w}} F^2 \left(u_+ c_+ + \frac{h^2}{12\eta} c_+^2 \right) \qquad [12]$$

where the first and second terms are the contributions from diffusive and convective fluxes caused by the electrostatic potential gradient. The second term appears because the slit is not electrically neutral.

Combining Equations 4 and Equations 9 thru 11 gives the electro-osmotic coefficient

$$\xi = \frac{-u_+ \frac{M_+}{M_{\mathrm{w}}} + c_{\mathrm{w}} \frac{h^2}{12\eta}}{u_+ + \frac{c_+ h^2}{12\eta}} \qquad [13]$$

The first terms in the numerator and denominator in Equation 13 are contributions from diffusion of water opposite the electric field and diffusion of cation with the electric field, respectively. The second terms in the numerator and denominator arise from the convective flux of the solution along the electric-field gradient.

Finally, the water-transport coefficient relates water transport in the absence of current, and connects to diffusivity in the membrane

$$\nabla \mu_{\mathrm{w}} = -\frac{RT}{D_{\mathrm{w}} c_{\mathrm{w}}} x_+ N_{\mathrm{w}} = -\frac{1}{\alpha} N_{\mathrm{w}} \qquad [14]$$

where R is the gas constant, T is temperature, D_{w} is the effective diffusivity of water in the membrane, and x_+ is the mole fraction of dissociated protons (4).

Equations 12 thru 14 relate nanoscale properties to network transport. We now turn to what these properties are. The fraction of protons dissociated from sulfonate groups is dictated by the hydration state of the membrane. As the membrane hydrates, water, $\mathrm{H_2O}$, solvates protons, $\mathrm{H^+}$, dissociating them from the sulfonate groups, $\mathrm{RSO_3^-}$,

$$(v_+ + v_-)\mathrm{H_2O} + \mathrm{HRSO_3} \rightleftharpoons \mathrm{H^+(H_2O)}_{v_+} + \mathrm{RSO_3^-(H_2O)}_{v_-} \qquad [15]$$

where v_+ and v_- are the number of water molecules solvating the proton and sulfonate group, respectively. The equilibrium constant, K, of Equation 15 is

$$K = \frac{\left[\mathrm{H^+(H_2O)}_{v_+}\right]\left[\mathrm{RSO_3^-(H_2O)}_{v_-}\right]}{[\mathrm{HRSO_3}][\mathrm{H_2O}]^{(v_+ + v_-)}} \qquad [16]$$

where the brackets denote thermodynamic activities. We assume that the activity of water outside ion solvation shells is unity and the other species are ideal. Thus, the fraction of dissociated protons is

$$f_+ = \frac{K(\lambda + v - 1) - \sqrt{K(4\lambda + K(1 + \lambda - v)^2)}}{2(K(v-1)-1)} \quad [17]$$

where $v = v_+ + v_-$ and is approximated as 4 (3). Consequently, a mass balance gives the fraction of water not solvating ions (i.e. free water)

$$f_{\mathrm{w}} = 1 - \frac{f_+ v}{\lambda} \quad [18]$$

for $\lambda > f_+ v$ and $f_{\mathrm{w}} = 0$ otherwise. The fraction of free water governs the water-transport coefficient, as shown in Table I, and is consistent with experiment (8). Values and expressions of additional nanoscale parameters are also given in Table I.

TABLE I. Nanoscale properties. Note: N_A is Avogadro's number

Property	Expression/Value	Units	Source/ Assumptions
Average water content	$\langle\lambda\rangle(\mu_{\mathrm{w}})$	-	Fit from (3)
Water volume fraction	$\varphi_{\mathrm{w}} = \frac{V_{\mathrm{w}}\lambda}{V_{\mathrm{w}}\lambda + EW/\rho_p^{\mathrm{dry}}}$	-	Ideal mixing
Proton mobility	u_+ =3.75E-12	s mol kg^{-1}	Infinite dilution (9)
Slit height	$h = (\lambda V_{\mathrm{w}}/N_A)^{\frac{1}{3}}$	m	Isotropic swelling
Solution viscosity	η = 8.90x10^{-4}	Pa s	Pure water (10)
Concentration of dissociated protons	$c_+ = f_+/V_{\mathrm{w}}\lambda$	mol m^{-3}	Ideal mixing and negligible proton volume
Concentration of water	$c_{\mathrm{w}} = 1/V_{\mathrm{w}}$	mol m^{-3}	Ideal mixing and negligible proton volume
Proton molar mass	M_+ = 1	g mol^{-1}	(10)
Water molar mass	$M_{\mathrm{w}} = 18$	g mol^{-1}	(10)
Water diffusivity	$D_{\mathrm{w}} = \varphi_{\mathrm{w}} f_{\mathrm{w}}$2.3 x10^{-9}	m^2 s^{-1}	Free water has diffusivity of bulk water (8)
Mole fraction of dissociated protons	$x_+ = f_+/(\lambda + f_+)$	-	Definition
Solvation equilibrium constant	$K = 0.30$	-	Fit Equation 17 to molecular-dynamics simulations (11)
Water molar volume	V_{w} = 1.8E-5	m^3 mol^{-1}	(10)
Polymer equivalent weight	$EW = 1100$	g polymer / mol SO_3^-	(3)
Density of dry polymer	ρ_p^{dry} = 2E-6	g m^{-3}	(3)

Simulations

Equations 12 thru 14 specify the transport properties of domains as a function of water content. Equations 7 and 8 are solved for ionic and water chemical potential for 15^3 nodes on a cubic grid. The grid spacing and, consequently, aqueous domain length, L, is 2 nm and each node has a coordination number (number of nodes connected to it) of three, consistent with experimental observations (12). The entire mesoscale simulation size is 30^3 nm^3. We use a simplified systems with square grids of 20^2 nodes for qualitative visualization of simulation results.

The water chemical potential at the top and bottom boundary nodes control the average water content of the network. The nodes at the back, front, left, and right sides are periodic (e.g. a left boundary node connects to a right opposing boundary node), thereby simulating an infinite sheet. A small fixed ionic potential drop (of 1×10^{-5} V) at the top and bottom nodes of the network determines the effective network conductivity, κ_{eff}, and electro-osmotic coefficient, ξ_{eff}. A small chemical-potential drop (equivalent to a 0.001% difference in relative humidity) simulates the water-transport coefficient of the network, α_{eff}. Such small driving forces assure obedience to linear transport laws. The effective transport properties are given by Equations 3 thru 5, where the current and water flux is the sum over the top (or, equivalently, bottom) face nodes and normalized by face area; the potential difference between the top and bottom nodes and the height of the network replaces 'Δ' and 'L,' respectively.

The system of 3375 equations was solved numerically using a modified Powell method in the SCIPY module of python 3.6. The relative tolerance was $1\text{x}10^{-12}$. The solution to the accompanying linear system of equations (i.e. Equations 7 and 8 with transport coefficients independent of chemical potential) provided the initial guess solution. The resistor-network geometry was constructed using OpenPNM (13).

We treat the difference from the mean of water content, e_λ, as a random variable for each domain with a normal distribution centered around zero. Negative values of λ were set to zero, slightly biasing $\langle\lambda\rangle$ higher than the measured value at a given water chemical potential. The standard deviation of the distributions, σ_λ, is equal to 7 (mole H_2O/mole HSO_3), unless otherwise stated.

Results and Discussion

Nanoscale Transport Properties

Figure 1 shows the nanoscale transport properties κ (solid line), ξ (dashed line), and α (dash-dot line) as a function of domain water content. The water-transport and electro-osmotic coefficients monotonically increase with hydration. At low water content, water molecules in a domain solvate the ions and have low mobility. Additional water is free and

rapidly diffuses and widens the aqueous domain, increasing the water-transport coefficient. Moreover, swelling of the aqueous domains causes increasing convection and electro-osmosis, as Equations 11 and 13 show. Similarly, conductivity increases markedly with water content at low hydrations because the hydrophilic volume fraction grows and protons dissociate from sulfonate groups. However, above $\lambda = 9$, water dilutes charge carriers, decreasing conductivity.

The probability distribution function of λ for three values of σ_D in Figure 1 emphasizes the heterogeneous water distribution. For $\sigma_\lambda = 7$, a membrane with $\langle\lambda\rangle = 14$ has both dry domains and those with more than twice the average water content. The hydrated domains have vastly larger transport coefficients than dry ones. σ_λ determines the shape of the water-content distribution.

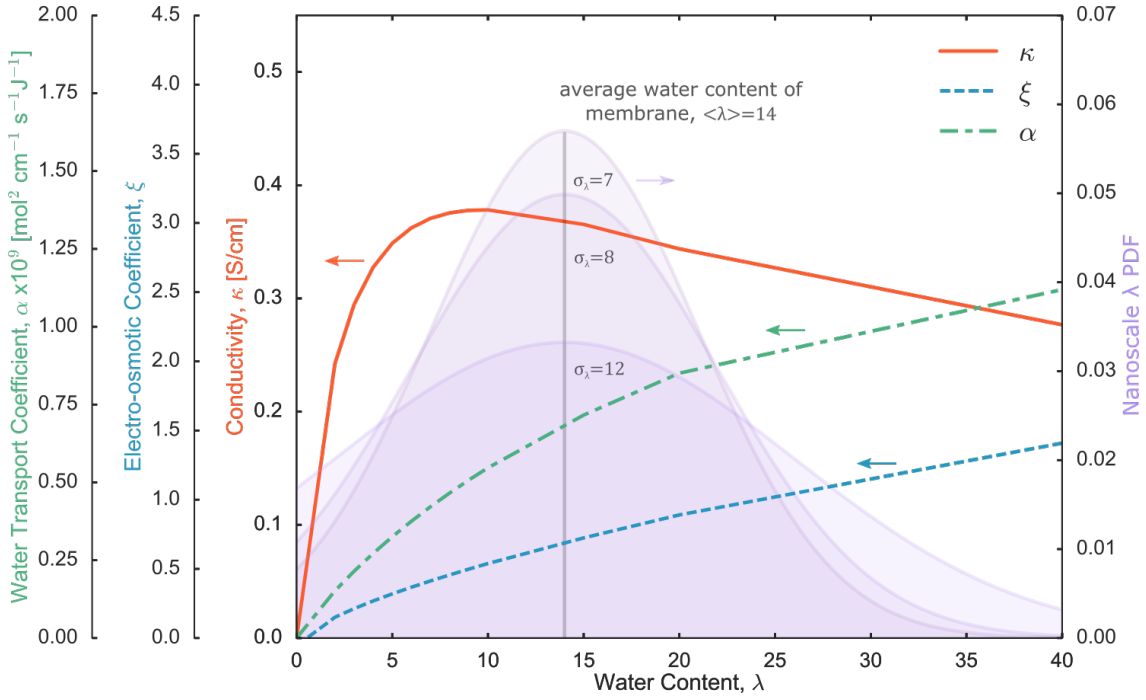

Figure 1. Nanoscale transport coefficients κ (solid line), ξ (dashed line), and α (dash-dot line) as a function of domain water content, λ. The shaded regions are probability distribution functions (PDFs) of λ with $\sigma_\lambda = 7, 8$, and 12 in a membrane with $\langle\lambda\rangle = 14$ (solid, grey, vertical line). Transport coefficient axes, are on the left; PDF axis is on the right.

Effective Transport Properties

Figure 2 shows the effective transport properties of the network κ_{eff} (solid line), ξ_{eff} (dashed line), and α_{eff} (dash-dot line) as a function of hydration. The predictions quantitatively match measured conductivity (squares) and show the same trend as experimental electro-osmotic (circle) and water-transport coefficients (diamonds) but with poor quantitative agreement. The lack of agreement stems from simplified nanoscale physics. For example, the electro-osmotic coefficient only accounts for the hopping

mechanism of proton transport and not the vehicular, which results in lower values (3). Moreover, electro-osmotic and water transport coefficients are notoriously difficult to measure without artifacts (3).

In contrast to nanoscale transport, all effective properties monotonically increase with increasing water content because of increasing network connectivity. At low hydration, water and protons only transport through the few connected, wet domains. With increasing $\langle\lambda\rangle$ wet domains progressively neighbor each other and provide additional transport pathways, increasing κ_{eff} and α_{eff}.

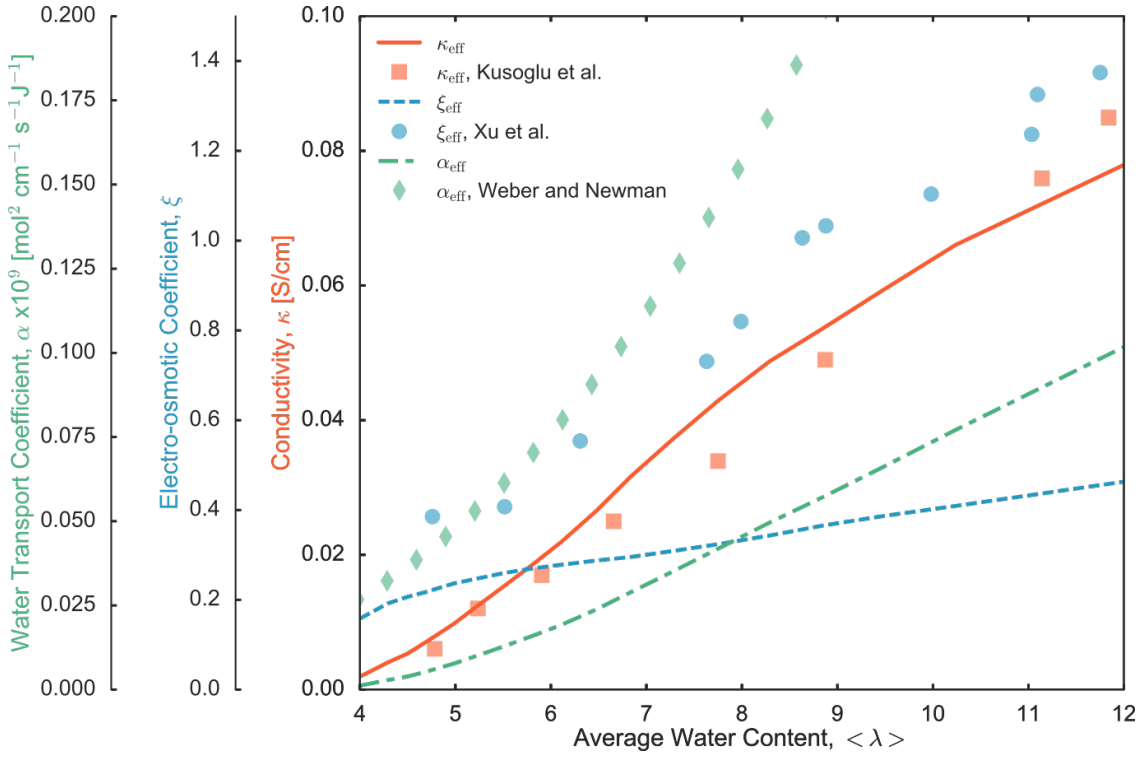

Figure 2. Effective network-transport coefficients from the model and experiments for κ_{eff} (model is solid line and experiments are squares (3)), ξ_{eff} (model is dashed line and measurements are circles (14)), and α_{eff} (model is dash-dot line and fit to experiments is diamonds (4)), as a function of average membrane water content, $\langle\lambda\rangle$.

The impact of network connectivity is not equal for all transport properties, however. Figure 3 shows that the effective network tortuosity, τ_X (defined as $\tau_X = X_{eff}/X$, where X is a transport property) is different for ion and water transport. The values of τ indicates the dominance of the mesoscale over the nanoscale. The insert in Figure 3 explores this relationship by showing simulation results of a 20x20 node square network with an applied potential across the top and bottom. Segments are black lines and colored spheres are nodes on the maximum flux path (i.e., a path starting from the middle node at the bottom boundary and following segments that carry the most flux out of each node on the path; these segments carry, on average, 90% of the flux from a node). The highest current and water pathways are colored red and green, respectively. Tan balls are shared maximum pathways for water and ions.

The insert in Figure 3 illustrates that τ_α is larger than τ_κ because water-transport pathways are longer. Similarly, τ_ξ is greater than one because the ratio of water to proton transport across a network is less than the ratio moving across an average domain. The variance of domain transport properties causes these different pathway lengths. For example, κ is relatively invariant with water content at high saturations. Consequently, the distribution of water in the membrane does not cause a heterogeneous conductivity distribution. In contrast, α has a heterogeneous network distribution because it depends strongly on hydration, as illustrated in Figure 1.

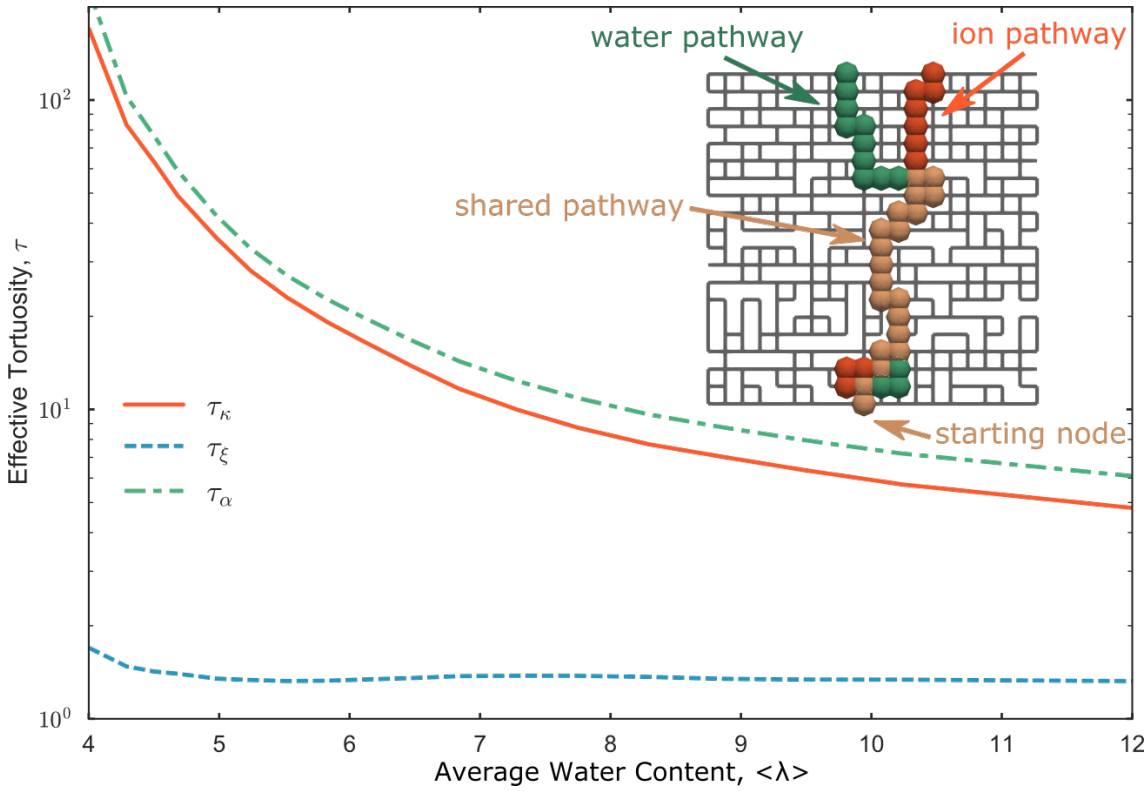

Figure 3. Effective network tortuosity, τ, for conductivity, κ (solid line), electro-osmotic coefficient, ξ (dashed line), and water-transport coefficient, α (dash-dot line), as a function of average network water content, $\langle\lambda\rangle$. Insert shows simulation results for a 20x20 node network. Segments are black lines. Red and green spheres show maximum ion current and water flux pathways, respectively, and shared pathways are tan.

Increasing network heterogeneity creates longer transport pathways and decreases effective transport properties. Figure 4 demonstrates that as the variance of domain water content, σ_λ, increases from 7 (sold line) to 8 (dashed line) and 12 (dash-dot line), κ_{eff} decreases. The insert provides visualization of the tortuous ion transport for more heterogeneous networks by showing the pathways of maximum flux for a 20x20 node network simulation with $\sigma_\lambda = 7$ (dark) and 12 (light). This result explains the higher experimental conductivity of membranes that are more homogeneous because of thermal treatments (squares) than untreated membranes (diamonds).

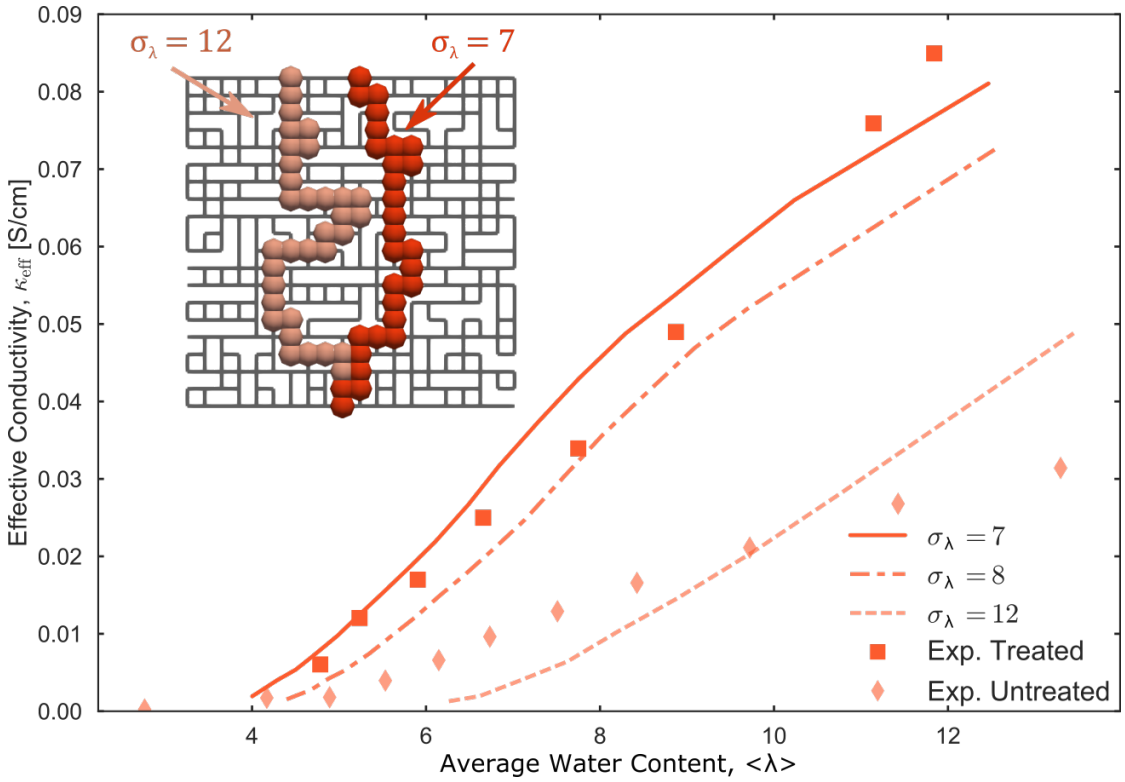

Figure 4. Effective network conductivity, κ_{eff}, for a network with the variance of water content, σ_λ, of 7 (solid line), 8 (dash-dot line), and 12 (dashed line). Insert shows simulation results for a 20x20 node network. Segments are black lines. Light ($\sigma_\lambda = 12$) and dark ($\sigma_\lambda = 7$) spheres are nodes along pathways of maximum current.

Summary

This paper connects nanoscale phenomena in PFSAs to macroscopic water and proton transport properties. Diffusion and electrokinetic transport of aqueous protons and water in a slit with charged walls establishes transport in PFSA domains as a function of local water content. For upscaling, a cubic resistor network represents the interconnected hydrophilic phase. The nanoscale model parameterizes the resistor-network element properties. Our network model bridges nanoscale and macroscale transport properties.

We show that macroscale properties emerge out of the mesoscale architecture of PFSAs. The effective conductivity and water-transport and electro-osmotic coefficients differ from nanoscale properties in both magnitude and hydration dependence. While nanoscale properties strongly depend on solvation of sulfonic-acid groups and domain size, mesoscale transport requires connections between wet regions. Moreover, effective connectivity is species dependent: water forms longer transport pathways through PFSAs than do protons. Even the coupling between water and proton transport (i.e. the electro-osmotic coefficient) is different for the network than for a single aqueous domain.

These insights into multiscale transport in PFSAs caution against attempts to interpret phenomena at disparate lengthscales in heterogeneous media without considering intermediary ones. Conversely, there are avenues for improving membrane performance that effect change at mesoscale (e.g., membrane thermal treatments). The proposed model guides exploration of these approaches and engineering of improved membranes.

Acknowledgements

This work was funded by the Assistant Secretary for Energy Efficiency and Renewable Energy, Fuel Cell Technologies Office, of the U. S. Department of Energy under contract number DE-AC02-05CH11231 and by a National Science Foundation Graduate Research Fellowship under Grant No. DGE 1106400.

References

1. A. Z. Weber, R. L. Borup, R. M. Darling, P. K. Das, T. J. Dursch, W. Gu, D. Harvey, A. Kusoglu, S. Litster, M. M. Mench, R. Mukundan, J. P. Owejan, J. G. Pharoah, M. Secanell, I. V. Zenyuk, *J. Electrochem. Soc.,* **161**, F1254 (2014).
2. J. Newman and K. E. Thomas-Alyea, *Electrochemical Systems,* chp. 9, John Wiley & Sons (2012).
3. A. Kusoglu and A. Z. Weber, *Chem. Rev.,* **117***,* 987 (2017).
4. A. Z. Weber and J. Newman, *J. Electrochem. Soc.,* **151**, A311 (2004).
5. P. Berg and M. Stornes, *Fuel Cells,* **16**, 715 (2016).
6. M. Sahimi, *Flow and Transport in Porous Media and Fractured Rock: From Classical Methods to Modern Approaches*, chp. 2, John Wiley & Sons (2012).
7. R. B. Bird, E. N. Lightfoot and E. W. Stewart, *Transport Phenomenon,* chp. 17, Wiley (2007).
8. Q. Berrod, S. Lyonnard, A. Guillermo, J. Ollivier, B. Frick, A. Manseri, B. Améduri and G. Gébel, *Macromolecules,* **48**, 6166 (2015).
9. C. G. Zoski, *Handbook of Electrochemistry*, p 935, Elsevier, (2006).
10. *CRC Handbook of Chemistry and Physics*, chp. 3, CRC Press, Cleveland, Ohio (1978).
11. R. Devanathan, N. Idupulapati, M. D. Baer, C. J. Mundy and M. Dupuis, *J. Phys. Chem. B,* **117**, 16522 (2013).
12. A. R. Crothers, C. J. Radke and A. Z. Weber, *ECS Trans.,* **69**, 731 (2015).
13. J. Gostick, M. Aghighi, J. Hinebaugh, T. Tranter, M. A. Hoeh, H. Day, B. Spellacy, M. H. Sharqawy, A. Bazylak, A. Burns, W. Lehnert, A. Putz, *Comp. Sci. & Eng.,* **18**, 60 (2016).
14. F. Xu, S. Leclerc, D. Stemmelen, J.-C. Perrin, A. Retournard and D. Canet, *J. Membr. Sci.,* **536**, 116 (2017).